Kovove Mater. 60 2022 223–231
DOI: 10.31577/km.2022.4.223

Investigation of microstructure evolution of Inconel 939 joint diffusion brazed using an amorphous liquated Ni-Cr-Fe-Si-B interlayer

Hamid Tazikeh, Seyyed Ehsan Mirsalehi*, Ali Shamsipur

Department of Materials and Metallurgical Engineering, Amirkabir University of Technology (Tehran Polytechnic), Tehran 15875-4413, Iran

Received 12 July 2021, received in revised form 19 June 2022, accepted 23 June 2022

Abstract

In this study, IN-939 high-chromium nickel-based superalloy was diffusion brazed using an amorphous Ni-Cr-Fe-Si-B foil as an interlayer and under high vacuum conditions. A successful joint was obtained at the applied temperature and bonding time of 1120 °C and 45 min. The microstructural evolution of the joint area was also investigated. The phases formed through the bonding process were categorized into three distinguished zones: isothermally solidified, athermally solidified, and diffusion-affected zones. According to the results, a gamma solid--solution single-phase was produced in the centerline of the joint. Also, some precipitates with blockage and Widmanstatten morphologies were observed in the diffusion-affected area that appears to be Cr-rich borides. Chromium depletion occurred in the gamma matrix adjacent to these precipitates. In addition, the number of precipitates decreased, moving away from the interface of the isothermally solidified zone towards the base metal. The highest and lowest microhardness values were obtained for the DAZ and ISZ, respectively. The precipitation of hard Cr-rich boride particles in the DAZ and the absence of a second phase in the ISZ microstructure were probably responsible for this difference in the hardness.

K e y w o r d s: diffusion brazing, Inconel 939, isothermal solidification, amorphous Ni-Cr-Fe--Si-B interlayer

1. Introduction

Nickel-based superalloys are broadly utilized in various sectors, especially in the aerospace and energy industries, because of their outstanding resistance to oxidation and significant creep behavior at high temperatures [1–3]. Among them, cast nickel-based high--chromium superalloys such as Inconel 939 (IN-939) have received much attention in different industries, such as aircraft components, chemical plant equipment, and petrochemical equipment, because of their extraordinary resistance to hot corrosion and oxidation. Considering the significant amounts of gamma-prime (γ') precipitates like aluminum and titanium presented in their chemical composition, this superalloy is strengthened by the distribution of gamma-prime precipitates gamma solid-solution matrix [3–6].

Previous studies showed that IN-939 is a strengthened superalloy of γ' precipitation that improved with a change in Waspaloy [4]. At the same time, precipitation-hardened nickel-based superalloys, like Waspaloy, be in the problematic category for welding due to the relatively high amounts of aluminum and titanium, which cause high susceptibility to crack in the heat-affected zone [5, 7]. In addition, IN-939 has inadequate welding capability due to its high sensitivity to microfissuring, especially in the so-called heat-affected zone during the welding process, because its chemical composition contains large amounts of γ constituents like aluminum and titanium [8, 9].

It has been found that the blades and vanes of gas turbines are under various types of in-service damage due to hard-working requirements, like wear, erosion, hot corrosion, oxidation, thermal-fatigue cracking, and so on, which cause their destruction [8]. In addition, the cost of producing superalloy components is very

*Corresponding author: tel.: +98 21 64542978; e-mail address: mirsalehi@aut.ac.ir

Table 1. Chemical composition (in wt.%) for the base metal and the filler alloy

	Ni	Cr	Co	Ti	W	Al	Ta	Nb	C	Mn	Zr	Fe	Si	B	Mo
Base metal (IN-939)	Bal.	22.1	18.8	3.7	2.0	1.9	1.2	0.95	0.15	0.1	0.1	0.1	0.04	0.01	0.08
Filler metal (MBF20)	Bal.	7.0	–	–	–	–	–	–	0.06	–	–	3.0	4.5	3.2	–

high and almost time-consuming. Consequently, several joining and repairing methods appear economically viable compared to the complete replacement of damaged/failed parts. The most critical processes for joining and improving superalloy components are fusion welding, brazing, and diffusion welding, generally used in the industry [10, 11]. However, brazing as a joining and repairing method for superalloy parts possesses fundamental weaknesses limiting their applications because melting point depressants like B, Si, and P are joined to brazing filler alloys to increase fluidity and reduce their liquidus temperature. The cooling step of the brazing method can result in the formation of centerline intermetallics, such as B, Si, and P, due to the segregation of melting point depressants during non-equilibrium eutectic solidification. Therefore, due to the positive segregation of melting point depressants at the cooling stage, the mentioned centerline intermetallic compounds are formed due to a non-equilibrium eutectic solidification of the liquid phase. The formed hard and brittle eutectic microconstituents in the centerline have destructive impacts on the joint efficiency, divided into three categories. They include a reduction in the mechanical properties, re-melting temperature, and corrosion/oxidation resistance of the joint. Solid-state joining, on the other hand, is a convenient diffusion bonding method that is capable of bonding similar and dissimilar materials. Accordingly, it is possible to create a suitable qualitative bond by dispersing atoms of two solid-state materials through high temperature and pressure. It is important to note that this solid-state diffusion bond gained more attention from various industries, such as aerospace and nuclear, due to its higher bond quality and strength. In addition, phase segregation and the brittle intermetallic compound are less visible than in other traditional joining methods. Therefore, this process does not apply to couples with stable oxide layers because they cannot be quickly joined [12, 13].

Transient liquid phase (TLP) bonding or diffusion brazing is another important diffusion-based method that differs from solid-state joining due to inserting a thin third interlayer between the base metals [14]. This thin interlayer, which usually has a lower melting point than the base material, causes a phase change within the joint area and the formation of a liquid phase. With the onset of the liquid phase formation within the bonding area, the bonding accelerates at the bonding temperature due to the increased interactions between the interlayers and the base material, which facilitates the dissolution process. Due to isothermal solidification, the diffusion process occurs inside and outside the joint area. It can lead to a high-strength bond and a melting temperature higher than the initial bond. When the isothermal solidification process is not completed (as in a brazing diffusion process), the resulting joint will have a lower melting temperature than its original state [15–18]. Therefore, it is essential to consider this point in the TLP process.

As mentioned above, IN-939 is used in many industries, such as jet engines, aircraft landing gear, power-generation equipment, and airframes. However, reports on IN-939 joining methods are limited to a few studies on preventing micro-fissure formation through the fusion welding process. However, the lack of comprehensive knowledge of the transient liquid phase bonding IN-939 results in the need for further studies in this field. An attempt has already been performed to construct a dissimilar joint of IN-738 and IN-939 using a bonding method called wide gap TLP. But so far, the TLP bonding has rarely been employed to join IN-939. Studying the bonding performance, microstructure characteristics, and mechanical behavior of IN-939 joints produced through TLP bonding is essential for developing an efficient bonding process for IN-939 superalloy components [8, 10]. Therefore, this study dealt with the TLP bonding of IN-939 superalloy via amorphous Ni-Cr-Fe-Si-B filler alloy as the interlayer. Then, the related microstructure behavior is systematically investigated through bonding. In addition, the Ni-Cr-B ternary phase diagram is used to study the mechanisms of phase formation in the solidification region.

2. Materials and methods

In this study, Inconel 939 (IN-939) superalloy and Ni-Cr-Fe-Si-B filler alloy form an amorphous foil (MBF20) 50 μm thick and are utilized as the base metal and interlayer, respectively. In this regard, Table 1 lists the chemical composition of the mentioned base metal and interlayer. The dimension of the test sample of $5 \times 10 \times 10\,\mathrm{mm}^3$ was prepared from the base metal ingot through EDM (electrical discharge machining). Afterward, the contacting surfaces of the samples were ground by SiC papers up to 800 grit to eliminate any oxide layers. The samples were cleaned

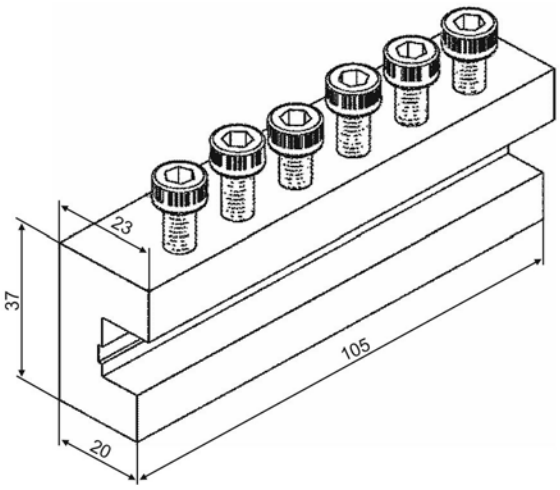

Fig. 1. Schematic representation of the manufactured holding fixture for restricting the sample movement and applying the desired pressure (all dimensions in mm).

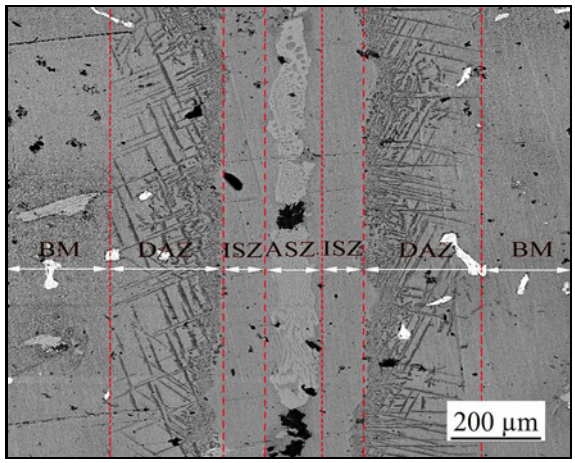

Fig. 2. SEM image of a diffusion brazing joint area describing the microstructure of three distinguished bonding regions of ASZ (athermally solidified zone), ISZ (isothermally solidified zone), and DAZ (diffusion affected zone). Also, BM is related to the base metal.

ultrasonically in the acetone bath to remove the contaminants from the surfaces before bonding. As shown in Fig. 1, a holding fixture (made of AISI 4140 steel) was designed and manufactured to fix the sandwich assembly after inserting the interlayer within two base metal samples. Also, the pressure was required to apply at the joint. Previous studies showed that it is unnecessary to implement external pressure on the joint because of the liquid phase in this kind of bonding. But, in some reports, the application of pressure was necessary to improve bonding. Hence, using the mentioned holding fixture, a pressure of 10 MPa was applied for this experiment [19].

Then, the loaded holding fixture was placed in the vacuum-type furnace at the pressure, temperature, and time of 1.33×10^{-2} Pa, 1120 ℃, and 45 min, respectively, to process the TLP bonding cycle. This temperature was utilized since it was below the solution temperature of the base metal (1160 ℃) and above the liquidus temperature of the filler metal (1103 ℃). Then, the loaded holding fixture was cooled to room temperature under vacuum conditions. After the experiment, the bonded samples were cut normal to the bond. In the following, the cross-sections were ground with SiC abrasive papers and polished with an alumina polishing slurry. Finally, they were etched for 30 s in Kalling's etchant, including 1 g copper chloride, 20 ml hydrochloric acid, and 20 ml ethanol. Afterward, scanning electron microscopic (SEM) analysis and semi-quantitative compositional analysis of the bonds were performed using a Tescan Mira3 field-emission SEM. This device was equipped with an energy dispersive X-ray spectrometer (EDS) that operated at an accelerating voltage and beam current of 15 kV and 1 nA, respectively. Also, Vickers microhardness (Hv) measurement was carried out on the brazed sample (bond region) under 25 g for the dwell time of 15 s.

3. Results and discussion

Figure 2 shows three distinguished bonding zones through the TLP of IN-939 at the applied temperature and holding time of 1120 ℃ and 45 min. They include athermally solidified zone (ASZ), isothermally solidified zone (ISZ), and diffusion affected zone (DAZ). The formation of these three distinct regions has also been observed in nickel-based superalloys with partial isothermal solidification after TLP bonding.

ASZ formation occurs when the bonding time is insufficient to complete isothermal solidification. This type of solidification is primarily driven by a decrease in temperature and relies more on the cooling period than diffusion. Some fluid phases remain in the joint centerline if the bonding time is insufficient to complete the isothermal solidification. After the liquid phase solidifies athermally, some intermetallic phases form at a eutectic reaction, destroying the mechanical strength and ductility. Also, ISZ develops through a phenomenon termed isothermal solidification. This type of solidification is driven by the inter-diffusion of MPD elements from the molten filler metal and base metal alloying elements. The whole solidification process occurs at a constant temperature known as the bonding temperature of diffusion brazing. If the bonding time is sufficient, the entire liquid phase is solidified isothermally so that no trace of residual liquids and eutectic micro-constituents is visible in the centerline. In addition, DAZ contains precipitates

with Widmanstatten/acicular and blocky morphologies that form in the base metal near the interface of ISZ and substrate. It should be noted that the formation of these precipitates is related to the diffusion of PMD elements like B in the MBF20 filler alloy to the adjacent base metal due to the excessive solubility of B in the base metal. As a result, the appearance of some mighty boride constituents in the adjacent base metal similar to Cr in the IN-939 alloy indicates the formation of boride precipitates during the bonding period.

According to Fig. 2, it can be seen that the white phases recognized in the microstructure image of the different bonds are considered the primary carbides of the base metal. The presence of these carbides has also been described previously by other researchers who have studied the IN-939 superalloy. In this regard, the chemical composition (at.%) of primary carbides examined is equal to 3.73 % Ni, 3.45 % Cr, 2.2 % Co, 4.5 % Al, 46.9 % Ti, 16.46 % Nb, 20.3, 9 % Ta, and 2.37 % W. This chemical composition is in good accordance with previous findings [8, 10], which show that these carbides are of the MC type, where M is mainly Ti.

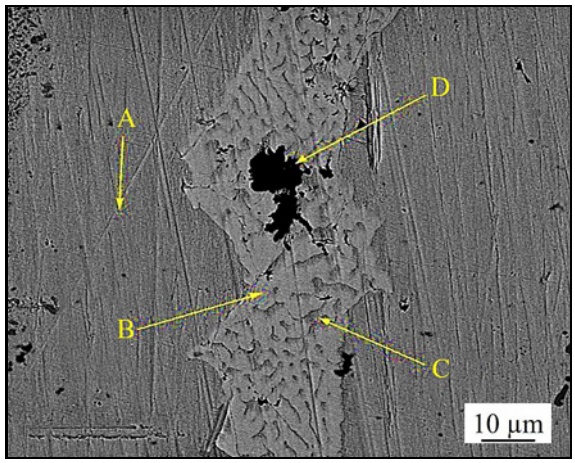

Fig. 3. Athermally solidified (ASZ) microstructure of the formed bond. A, B, C, and D indicate the primary gamma, the Ni-rich boride, the eutectic-gamma solid solution, and the Cr-rich boride, respectively.

Table 2. The EDS results in the chemical composition of the phases A, B, C, and D in the ASZ of the formed bond

Phase	Probable composition	Ni	Cr	Co	Al	Ti	Nb	Ta
A	Primary-gamma	65.47	13.61	6.02	2.93	1.42	0.4	0.42
B	Ni-rich boride	76.07	3.89	5.85	1.7	7.65	2.04	1.05
C	Eutectic-gamma	70.94	10.36	4.54	1.08	1.25	0.16	0.39
D	Cr-rich boride	2.43	86.63	0.31	1.51	1.06	0.82	0.63

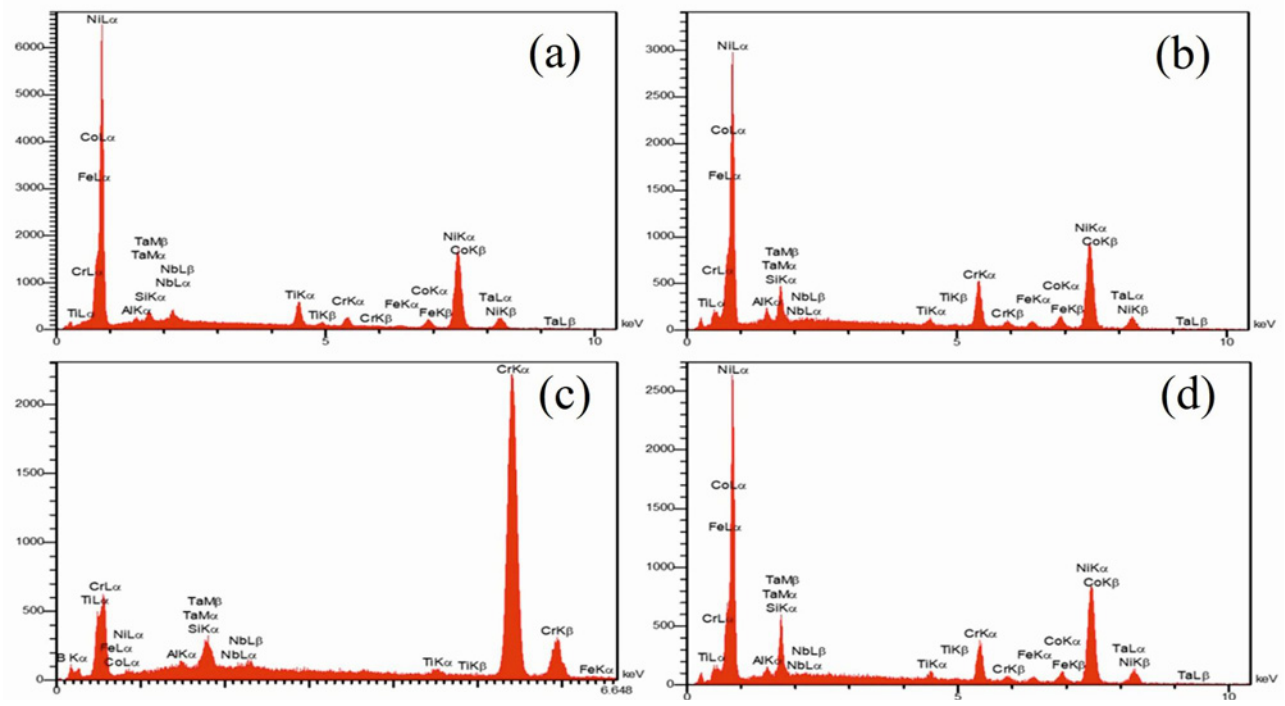

Fig. 4. The FESEM-EDS spectra of (a) the Ni-rich boride, (b) primary-gamma, (c) the Cr-rich boride, and (d) the eutectic-gamma solid-solution presented in Fig. 3.

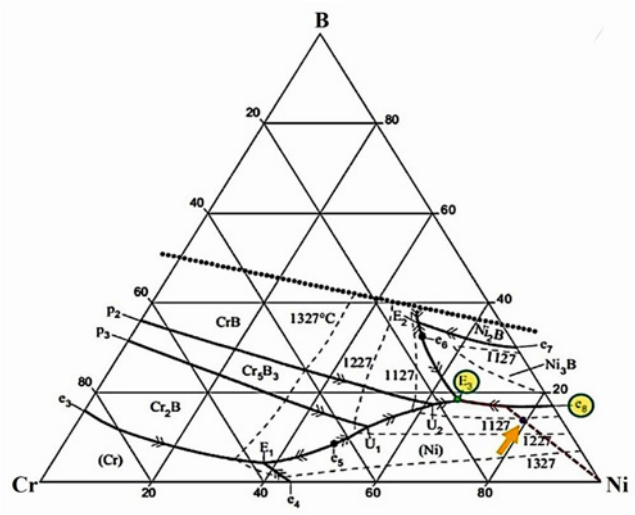

Fig. 5. Liquidus projection of the Ni-Cr-B ternary phase diagram [8]. The initial chemical composition of the filler metal is shown with the arrow.

Phases A to D are visible in the centerline microstructure obtained at the temperature of 1120 ℃ and lasting 45 min. As can be observed in this figure, the ASZ microstructure is composed of eutectic microconstituents elongated along the centerline. Therefore, this region consists of four separate phases with different chemical compositions, shown in Fig. 4 and Table 2. The B element can be detected in the intermetallic phases. Still, X-ray absorption from the analyzer window makes it difficult to quantify the light elements accurately.

The critical point is that the liquid phase will remain in the centerline until the isothermal solidification has been completed. The solidification of the remaining liquid begins directly after cooling from the bonding time. Based on the Ni-Cr-B ternary phase diagram shown in Fig. 5, the first phase to form near the ISZ will be the primary solid solution of the nickel-rich gamma. The segregation of alloy elements associated with solidification caused by cooling is the main factor that should be considered. Furthermore, the fabrication of the primary gamma as a pro-eutectic phase results in the emission of dissolved elements like boron, titanium, niobium, tungsten, and tantalum in the liquid phase. Primary-gamma growth is associated with dendritic morphology in these elements, which have a distribution coefficient of less than one [8, 14, 20]. Also, the maximum solubility of B in Ni occurs at 1087 ℃ (0.3 at.%). In addition, the distribution coefficient B in Ni can be calculated through the ratio between the specific heat of the solid phase (C_s) and liquid phase (C_l), and the Ni-B binary phase diagram. In this relationship, C_s combines solid equilibrium at eutectic temperature (T_{eu}), and C_l is the composition of liquid equilibrium at T_{eu}. As a result, its value equals 0.018, less than one.

The low solubility limit of B in Ni and the distribution coefficient (< 1) cause the B to be rejected in the residual liquid by solidifying the pro-eutectic phase. Also, B enrichment in the liquid phase proceeds with the fabrication of the primary gamma, as shown in Fig. 5. Once the concentration of B in the primary gamma reaches the solubility limit of B in the gamma phase, no primary-gamma phase can be solidified from the liquid phase. At this level, the chemical composition of the liquid reaches a eutectic composition, where it intercepts the solidification path of the binary eutectic line at 1042 ℃, see *e8*. The residual liquid is converted to a eutectic-gamma solid solution and a Ni-rich boride phase through a eutectic reaction. The solidification path pursues the *e8* eutectic line. Then, by forming two eutectic-gamma and nickel-rich boride phases, Cr rejects the remaining liquid.

Interestingly, the Cr enrichment of the residual liquid is related to the relatively low solubility of Cr in gamma solid-solution and Ni-rich boride. According to E3 in Fig. 5, it is also understood that lowering the temperature and Cr enriching the liquid leads the liquid phase composition to the ternary eutectic composition. After reaching the solidification path at point E3 (997 ℃), the three eutectic-gamma solid-solution, nickel-rich boride, and a Cr-rich boride form through a ternary eutectic reaction of the remaining liquid. After the ternary eutectic reaction at point E3, the solidification procedure ends. Previous studies have shown the fabrication of the same phases in the ASZ of other diffusion brazing bonded nickel-based superalloys utilizing Ni-Cr-B coatings. Based on Table 2 and the figures above, it can be inferred that phases "B," "C," and "D" are expected respectively to be nickel-rich boride, eutectic-gamma solid-solution, and Cr-rich boride. Based on the ternary phase diagram of Ni-Cr-B and the study of other researchers, "A" indicates a region where the amount of the primary-gamma phase is significant.

It should be noted that the primary-gamma phase amount is a fraction and is not easily detectable at the ASZ microstructure for two reasons. The first reason is the small volume fraction of the pro-eutectic phase because of the initial chemical composition of the filler metal to the binary eutectic line. Another reason is the small width of the residual liquid and ASZ because the thickness of the initial bond gap is very thin.

Subsequently, the dominant solidification mechanism in each region was studied to determine the phases formed in the bonding region through diffusion brazing IN-939 bonding. As mentioned earlier, isothermal solidification is the only governing solidification mechanism in the ISZ region [10, 12]. Liquid filler metal can experience significant compositional differences due to the diffusion of B from the molten filler metal to the near base metal. According to the Ni-B binary phase diagram, the liquidus temperature

Table 3. EDS results showing the chemical composition (in at.%) of the ISZ

Probable composition	Ni	Cr	Ta	Co	Al	Ti	Nb
Eutectic-gamma	71.73	12.6	4	3.7	2.9	0.5	0.2

increases with the depletion of the liquid filler metal from B. It means that the liquidus temperature gradually increases due to the diffusion of B from the liquid filler metal to the base metal. Isothermal solidification begins at the solid/liquid interface and proceeds to the centerline when the liquidus temperature reaches the bond temperature and reaches the centerline. It is mentioned that the influence of diffusion of alloying elements on the liquidus temperature relies on the coefficient of distribution of these elements. Therefore, these two phenomena increase liquidus phase temperature through isotherm solidification. The first case concerns reducing the liquid phase from MPD elements with values of j less than one. The second issue involves enriching the liquid phase with elements like Cr, Co, and W with values greater than one.

Considering no temperature drop occurs through isothermal solidification, there will be no solute rejection at the interface of solid/liquid. Hence, while preventing the enrichment of the liquid phase with any solute elements, the chemical composition of the liquid phase does not reach the eutectic composition. Consequently, secondary phases and eutectic products cannot develop. In this case, the single-phase gamma solid solution will be the only phase formed in the ISZ region. In this regard, Table 3 lists the chemical composition of the ISZ phase, which is connected to the microstructure of the diffusion brazing bond created at an applied temperature and time of 1120 ℃ and 45 min, respectively. Ni-rich gamma solid-solution based on the Ni-Cr-B ternary phase diagram and the initial composition of the Ni-Cr-Fe-Si-B filler metal appears to be the only phase formed in the ISZ region at this bond temperature.

According to the well-known TLP bonding theory, the base metal dissolution happens after the interlayer melts to reach equilibrium at the interface of solid/liquid. An important point to note in Table 3 is the presence of base metal alloying elements like cobalt, aluminum, titanium, niobium, and tantalum in ISZ, which are not present in the initial composition of the filler metal. The presence of these elements in ISZ is not only a confirmation of the diffusion of base metal elements in the liquid interlayer through the bonding cycle but also proof of the dissolution of the base metal in the first step of the TLP bonding process. Another sign of the base metal dissolution is the size of the widened gap of the bonded samples. In this regard, the distance between the two interfaces of DAZ/ISZ is supposed to be the maximum width

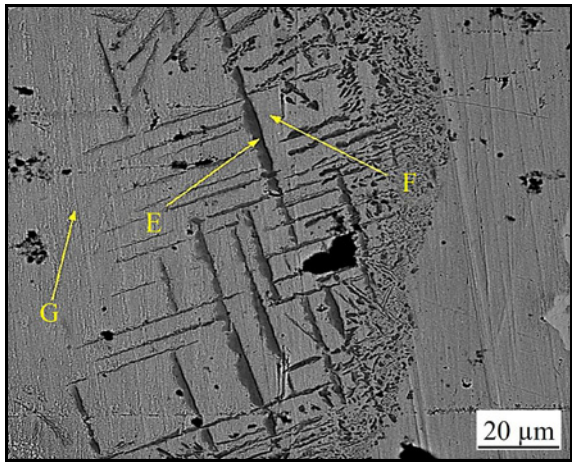

Fig. 6. SEM image of the DAZ microstructure of the formed bond, E: Acicular boride precipitates, F: Adjacent gamma-matrix of borides, G: matrix far from the DAZ borides.

of the liquid phase at the end of the base metal dissolution step. The size of the solidified zone appears to be larger than the size of the initial gap. This phenomenon is referred to as melt back, and in binary systems, the degree of melt back depends on the solidus and liquidus equilibrium diagrams at the bond temperature.

The formed DAZ microstructure corresponding to Fig. 2 is shown in Fig. 6. According to this figure, this region contains second phases with two blocks and acicular morphologies distributed in the matrix. The precipitates with block morphology generally form near the interface of ISZ/substrate and change to acicular/Widmanstatten morphology as they move away from the interface. Table 4 lists the chemical composition of the second phase of the DAZ region. The results show that DAZ precipitates are rich in Cr and B and lean in C. According to the chemical composition reported in Table 4, these precipitates appear to be Cr-rich borides. Two mechanisms can be used to interpret boride precipitation in DAZ. DAZ boride precipitates are formed at the solid/liquid interface before reaching equilibrium based on the first mechanism. It means that they are formed before the dissolution step is completed. This mechanism also implies that DAZ boride precipitates neither through the cooling cycle nor before the start of interlayer melting. The second process relates boride precipitates to the diffusion of B atoms from the liquid filler metal to the substrate

Table 4. EDS results showing the chemical composition (at.%) of phases in Fig. 6.

Phase	Probable composition	Ni	Cr	Co	Al	Ti	Nb	Ta
E	Cr-rich boride	7.04	84.86	4.61	1.12	1.15	0.44	0.7
F	Gamma phase close to the precipitation	51.22	18.39	19.22	5.9	3.74	0.61	0.7
G	Gamma phase far away the precipitation	45.78	26.09	18.77	5.21	2.99	0.45	0.6

during the isothermal solidification step that follows equilibration.

As shown in Fig. 6, more than 90 % of boride precipitates are seen at a distance of up to 45 μm from the interface of ISZ/substrate. At distances significantly greater than 45 μm, the microstructure of the base metal appears to be almost devoid of borides. Accordingly, B precipitates form in the substrate as the B concentration overpasses the solubility limit of base metal B (CBM). Therefore, it can be concluded that in the bond made in Fig. 6, by moving away from the ISZ/BM interface to the base metal, at a distance of up to 45 μm, the concentration of B gradually decreases to CBM. At distances greater than 45 μm, B concentration is lower than CBM. Therefore, there is no additional B element to react with the boride constituents like Cr, Nb, and W, and the boride precipitate is eliminated. Also, the peak seen in Fig. 6 in DAZ can be attributed to the accumulation of boride phases near the ISZ/substrate interface. In fact, in the presence of Cr in IN-939, a strong boride, notable B content is bound in the vicinity of the ISZ/substrate interface. Hence, only a few B atoms can be diffused over long distances. This issue could clarify how the amount of the precipitate of Cr-rich boride decreases gradually as the ISZ/BM interface moves away from the base metal. Previous studies on IN-718 and IN-738 agree with these findings [8, 16, 20].

Figure 7 presents an EDS X-ray elemental map of the DAZ precipitates. This figure indicates that DAZ precipitates are rich in chromium and lean in Ni and Co. It suggests the formation of Cr-rich boride precipitates in the DAZ and shows a decrease in Cr in the vicinity of the DAZ precipitates. According to Table 4, the Cr concentration of Cr-rich boride phases is higher than the Cr concentration of the adjacent matrix, indicating that precipitation of boride phases drives Cr consumption in the vicinity of DAZ precipitates. As a result of this consumption, Cr is reduced in the adjacent gamma matrix. Since Cr is the most prominent element in the corrosion resistance of IN-939, its reduction around DAZ precipitates can lead to susceptibility to corrosion attacks in these areas.

Figure 8 shows the average microhardness in various bonding regions of the brazed sample. As can be seen, four different regions are identified in the hardness profile. It should be mentioned that each region describes a specific microstructural zone. In the ASZ,

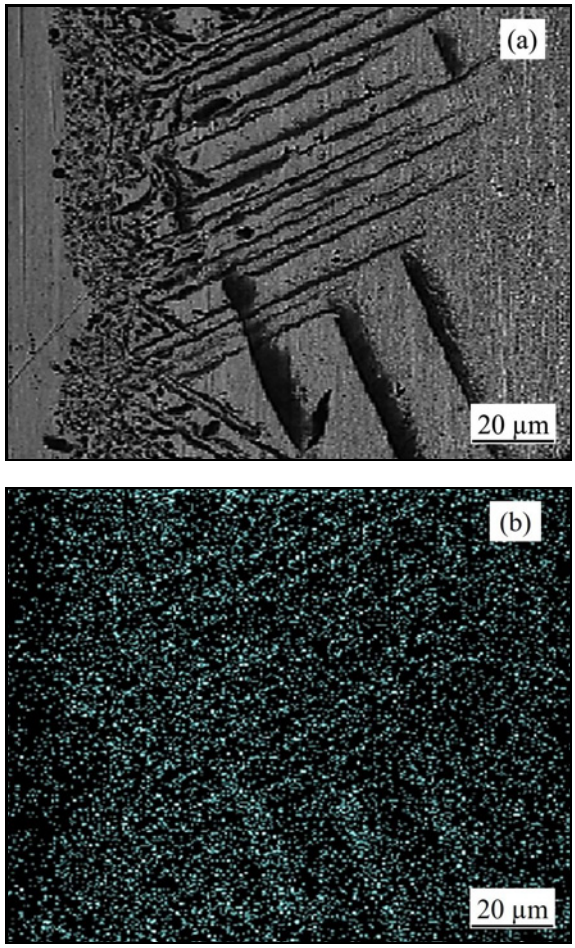

Fig. 7. EDS X-ray elemental distribution map of DAZ precipitates for Cr element (b) and the corresponding SE micrograph (a).

high hardness Ni-rich and Cr-rich borides along the centerline of the joints with incomplete isothermal solidification can demonstrate the high value of average microhardness. The local and non-continuous Cr-rich boride phase, compared to the prevailing Ni-rich boride phase at ASZ, has a less negative effect on joint performance. Thus, the microhardness line is passed only through the Ni-rich boride phase to measure the ASZ hardness.

According to Fig. 8 for the ISZ, it can be said that the average microhardness is even lower than that of the BM. In this regard, solid-solution hardening is pos-

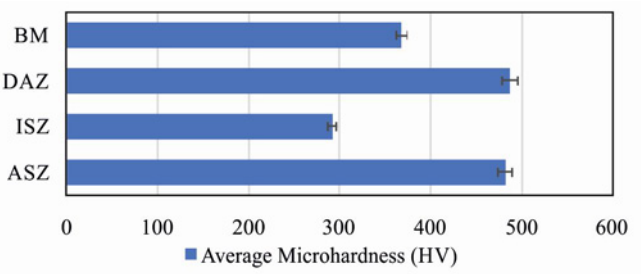

Fig. 8. The joint area's average microhardness (HV) value in different ASZ, ISZ, DAZ, and BM microstructural regions.

sible in this zone because of the second phase's absence in the mentioned microstructure. The interdiffusion of solute elements between the base metal and the interlayer controls the ISZ hardness. The lower hardness of ISZ compared to the BM can be attributed to two significant reasons. The first reason is related to the high concentrations of solid-solution strengthening elements such as Cr, Co, Al, and Ti in the base metal and insufficient diffusion of solute elements from the base metal into the ISZ. The second reason is the precipitation of a large fraction of γ' in the base metal. It can be concluded that the inadequate interdiffusion of solid-solution strengthening elements and γ' formers into this region is the main reason for the lower hardness of ISZ as compared to that of the BM.

For the BM region, the corresponding hardness is influenced by two hardening mechanisms of solid-solution and precipitation through the γ' precipitates in the γ-matrix. The microhardness profile approaches its highest value at DAZ due to the formation of Cr-rich boride particles in this region. The boride precipitates possess a rigid and brittle structure, leading to the increment of DAZ hardness compared to that of both ISZ and BM.

4. Conclusions

The Inconel 939 superalloy was successfully joined using an MBF20 amorphous foil as the interlayer using the diffusion brazing process. The phase formation and microstructural evolution during the isothermal solidification were investigated in different bonding regions. The most important results of this research can be expressed as follows:

– According to the observations, the formed phases can be categorized into three distinguished zones entitled isothermally solidified, athermally solidified, and diffusion-affected zones.

– The isothermal solidification phenomenon through diffusion brazing occurred at the applied temperature and bonding time of 1120 ℃ and 45 min. Accordingly, an intermetallic-free centerline, including a gamma solid-solution single-phase, was successfully obtained.

– Inadequate bonding time leads to some athermal solidification and the formation of primary-gamma and eutectic micro-constituents consisting of Ni-rich boride, eutectic gamma solid-solution, and Cr-rich boride.

– Chromium-rich boride precipitates were detected in the DAZ of the bond. Also, chromium depletion can be recognized in the gamma matrix adjacent to these precipitates. The precipitates decreased, moving away from the ISZ interface towards the BM.

– The highest microhardness value was obtained for the DAZ. The precipitation of hard Cr-rich boride particles in the DAZ was probably the main reason for the high hardness value of this region. The average microhardness of the ISZ was even lower than that of the BM, considering the absence of the second phase in its microstructure.

References

[1] H. Esmaeili, S. E. Mirsalehi, A. Farzadi, Vacuum TLP bonding of Inconel 617 superalloy using Ni-Cr-Si-Fe-B filler metal: Metallurgical structure and mechanical properties, Vacuum 152 (2018) 305–311. https://doi.org/10.1016/j.vacuum.2018.03.048

[2] J. Zhu, A. Wise, T. Nuhfer, G. R. Holcomb, P. D. Jablonski, S. Sridhar, D. E. Laughlin, High-temperature-oxidation-induced ordered structure in Inconel 939 superalloy exposed to oxy-combustion environments, Mater. Sci. Eng. A 566 (2013) 134–142. https://doi.org/10.1016/j.msea.2012.12.074

[3] A. Malekan, M. Farvizi, S. E. Mirsalehi, N. Saito, K. Nakashima, Influence of bonding time on the transient liquid phase bonding behavior of Hastelloy X using Ni-Cr-B-Si-Fe filler alloy, Mater. Sci. Eng. A 755 (2019) 37–49. https://doi.org/10.1016/j.msea.2019.03.124

[4] K. D. Ramkumar, W. S. Abraham, V. Viyash, N. Arivazhagan, A.M. Rabel, Investigations on the microstructure, tensile strength and high temperature corrosion behaviour of Inconel 625 and Inconel 718 dissimilar joints, J. Manuf. Process. 25 (2017) 306–322. https://doi.org/10.1016/j.jmapro.2016.12.018

[5] L. X. Zhang, Z. Sun, Q. Xue, M. Lei, X. Y. Tian, Transient liquid phase bonding of IC10 single crystal with GH3039 superalloy using BNi2 interlayer: Microstructure and mechanical properties, Mater. Des. 90 (2016) 949–957. https://doi.org/10.1016/j.matdes.2015.11.041

[6] M. A. Arafin, M. Medraj, D. P. Turner, P. Bocher, Transient liquid phase bonding of Inconel 718 and Inconel 625 with BNi-2: Modeling and experimental investigations, Mater. Sci. Eng. A 447 (2007) 125–133. https://doi.org/10.1016/j.msea.2006.10.045

[7] G. P. Dinda, A. K. Dasgupta, J. Mazumder, Laser aided direct metal deposition of Inconel 625 superalloy: Microstructural evolution and thermal stability,

Mater. Sci. Eng. A 509 (2009) 98–104. https://doi.org/10.1016/j.msea.2009.01.009
[8] F. Arhami, S. E. Mirsalehi, A. Sadeghian, Effect of bonding time on microstructure and mechanical properties of diffusion brazed IN-939, J. Mater. Process. Technol. 265 (2019) 219–229. https://doi.org/10.1016/j.jmatprotec.2018.10.021
[9] F. Arhami, S. E. Mirsalehi, The effect of heat treatment sequence on microstructure and mechanical properties of diffusion brazed IN-939 superalloy, J. Mater. Process. Technol. 266 (2019) 351–362. https://doi.org/10.1016/j.jmatprotec.2018.11.020
[10] M. Pouranvari, A. Ekrami, A. H. Kokabi, Microstructure development during transient liquid phase bonding of GTD-111 nickel-based superalloy, J. Alloys Compd. 461 (2008) 641–647. https://doi.org/10.1016/j.jallcom.2007.07.108
[11] M. Khakian, S. Nategh, S. Mirdamadi, Effect of bonding time on the microstructure and isothermal solidification completion during transient liquid phase bonding of dissimilar nickel-based superalloys IN738LC and Nimonic 75, J. Alloys Compd. 653 (2015) 386–394. https://doi.org/10.1016/j.jallcom.2015.09.044
[12] M. Pouranvari, A. Ekrami, A. H. Kokabi, Solidification and solid state phenomena during TLP bonding of IN718 superalloy using Ni-Si-B ternary filler alloy, J. Alloys Compd. 563 (2013) 143–149. https://doi.org/10.1016/j.jallcom.2013.02.100
[13] A. Y. Shamsabadi, R. Bakhtiari, G. Eisaabadi B., TLP bonding of IN738/MBF20/IN718 system, J. Alloys Compd. 685 (2016) 896–904. https://doi.org/10.1016/j.jallcom.2016.06.185
[14] F. Arhami, S. E. Mirsalehi, A. Sadeghian, M. H. Johar, The joint properties of a high-chromium Ni-based superalloy made by diffusion brazing: Microstructural evolution, corrosion resistance and mechanical behavior, J. Manuf. Process. 37 (2019) 203–211. https://doi.org/10.1016/j.jmapro.2018.11.025
[15] A. Ghoneim, O. A. Ojo, Numerical modeling and simulation of a diffusion-controlled liquid-solid phase change in polycrystalline solids, Comput. Mater. Sci. 50 (2011) 1102–1113. https://doi.org/10.1016/j.commatsci.2010.11.008
[16] B. Binesh, A. Jazayeri Gharehbagh, Transient liquid phase bonding of IN738LC/MBF-15/IN738LC: Solidification behavior and mechanical properties, J. Mater. Sci. Technol. 32 (2016) 1137–1151. https://doi.org/10.1016/j.jmst.2016.07.017
[17] M. A. González, D. I. Martínez, A. Pérez, H. Guajardo, A. Garza, Microstructural response to heat affected zone cracking of prewelding heat-treated Inconel 939 superalloy, Mater. Charact. 62 (2011) 1116–1123. https://doi.org/10.1016/j.matchar.2011.09.006
[18] A. Doroudi, A. Shamsipur, H. Omidvar, M. Vatanara, Effect of transient liquid phase bonding time on the microstructure, isothermal solidification completion and the mechanical properties during bonding of Inconel 625 superalloy using Cr-Si-B-Ni filler metal, J. Manuf. Process. 38 (2019) 235–243. https://doi.org/10.1016/j.jmapro.2019.01.019
[19] F. Arhami, S. E. Mirsalehi, Microstructural evolution and mechanical properties evaluation of IN-939 bonds made by isothermal solidification of a liquated Ni-Cr-B interlayer, Metall. Mater. Trans. A Phys. Metall. Mater. Sci. 49 (2018) 6197–6214. https://doi.org/10.1007/s11661-018-4918-3
[20] A. Sadeghian, F. Arhami, S. E. Mirsalehi, Phase formation during dissimilar transient liquid phase (TLP) bonding of IN939 to IN625 using a Ni-Cr-Fe-Si-B interlayer, J. Manuf. Process. 44 (2019) 72–80. https://doi.org/10.1016/j.jmapro.2019.05.027